Baghdad Science Journal

Volume 23 | Issue 6 Article 13

6-22-2026

Modeling and Performance Analysis of Two-Dimensional VCSEL Using Finite Element Simulation

Rand Mahdi Khudair
Department of Physics College of Science for Women, University of Baghdad, Baghdad, Iraq, rand.abbas1704@csw.uobaghdad.edu.iq

Shaimaa S. Mahdi
Department of Physics College of Science for Women, University of Baghdad, Baghdad, Iraq, shaimaa.saleh@CSW.uobaghdad.edu.iq

How to Cite this Article

Khudair, Rand Mahdi and Mahdi, Shaimaa S. (2026) "Modeling and Performance Analysis of Two-Dimensional VCSEL Using Finite Element Simulation," *Baghdad Science Journal*: Vol. 23: Iss. 6, Article 13.
DOI: https://doi.org/10.21123/2411-7986.5327

BAGHDAD SCIENCE JOURNAL 2026;23(6):2117–2127

Scan the QR to view the full-text article on the journal website

RESEARCH ARTICLE

Modeling and Performance Analysis of Two-Dimensional VCSEL Using Finite Element Simulation

Rand Mahdi Khudair *, **Shaimaa S. Mahdi**

Department of Physics College of Science for Women, University of Baghdad, Baghdad, Iraq

ABSTRACT

Vertical cavity surface emission lasers (VCSELs) are considered to be an integral component of short-range optical communication. Compact structure, low threshold current, and high modulation capability are the reasons why these communication systems are used. efficiency. This study presents a two-dimensional numerical simulation of a VCSEL structure at a wavelength of 850 nm using the finite element method (FEM) via Laser MOD software to investigate the effect of using two different quantum well materials (QW) GaAs, and AlGaAs on the optical performance of the device. All of the above were done within the same cavity and DBR structure to provide a consistent comparison. The results indicate that the optical gain of GaAs is higher, around 400 cm^{-1}, than AlGaAs which has a lower optical gain of around 350 cm^{-1}. GaAs also operates at a lower threshold current of approximately 0.45 mA, compared to AlGaAs, which operates at a threshold current of 0.67 mA. Thermal analysis shows that the self-heating effect begins at a lower temperature in the AlGaAs structure, around 350 K, compared to GaAs, which can operate stably up to approximately 375 K due to its high thermal conductivity. In general, the comparison illustrates the balance between performance, gain, and optical confinement of the two materials under the same structural and thermal conditions.

Keywords: Distributed bragg reflector (DBR), Finite element method (FEM), Near field intensity, Optical mode power, Quantum well

Introduction

The spread of technology and information transmission via optical fibers and sensors has led to many devices. This requires these devices to operate at high speeds and remain stable at high temperatures. Therefore, vertical cavity surface-emitting lasers (VCSELs) were introduced to the laser market and have achieved remarkable success due to their advantages over other lasers, such as high efficiency, significantly lower production costs, small size, low threshold currents, and many other features that enable them to be used in a wide variety of applications.[1–3] In the early 1980s, the VCSEL laser at a wavelength of 850 nm was used as a light source for short-range communications, replacing edge-emitting lasers. This is because VCSELs offer high coupling efficiencies with optical fibers and also have single-mode operation due to their small cavity. In addition, the current development of the Internet has created an urgent need to improve and develop new VCSEL designs.[4–7] The process of exploring new VCSEL designs requires facing numerous upgrades to achieve improved and highly efficient VCSEL devices. For this reason, advanced computer-aided design (CAD) tools will play a significant role, as they provide essential support for designing prototypes. This step eliminates the cost of expensive pilot manufacturing processes.[8–10] Given the high cost of manufacturing VCSEL prototypes and the lack of scientific expertise, numerical simulation

Received 13 August 2025; revised 16 March 2026; accepted 11 April 2026.
Available online 22 June 2026

* Corresponding Author.
E-mail addresses: rand.abbas1704@csw.uobaghdad.edu.iq (R. M. Khudair), shaimaa.saleh@csw.uobaghdad.edu.iq (S. S. Mahdi).

https://doi.org/10.21123/2411-7986.5327

and modeling are critical for designing advanced, high-performance devices. These processes can also design improved structures with desirable properties and provide a comprehensive understanding of the physical and structural processes of the device, such as wavelength and optical infrastructure design. Maxwell's equations must also be solved accurately to arrive at accurate results for the electromagnetic field. Many different numerical simulations have been used, including the finite element method the finite integration technique (FIT), the finite-difference time-domain (FDTD) method, and the precision coupled wavelet analysis (RCWA). All of these techniques have been developed and used in Nano-optical simulations.[11–14] In 2024, a VCSEL operating at 850 nm with an oxide aperture of about 11 μm was designed and validated based on the temperature-dependent effects on the output characteristics such as threshold current, bandwidth, and optical output power.[10] In the same year, another study addressed the development of a high-power, high-efficiency VCSEL operating at 980 nm. Simulations and experiments demonstrated improved modulation capability and efficiency. A VCSEL with a 6 μm oxide aperture was fabricated, achieving an efficiency of 42%.[15] This research investigates the optical and thermal behavior of VCSEL devices based on AlGaAs/GaAs quantum wells within a specific design architecture. A comparative analysis of threshold current, optical spectrum, and output power characteristics is carried out under varying temperature conditions. The results help clarify how the choice of quantum well material influences the device performance and provide useful insights for improving low-threshold VCSEL operation.

Materials and methods

Methodology

Optical confinement and detectable laser light intensity in VCSELs were achieved using distributed Bragg reflectors (DBRs), which are multilayers with successively high and low refractive indices. Each layer is a quarter-wavelength thick to achieve constructive interference, where DBR is the wavelength obtained from the multi-quantum well (MQW) region[16,17] which is a thin layer of material with a specific bandwidth used to increase the interaction efficiency between electrons and photons, leading to improved photocatalysis in optical devices such as VCSELs. The light intensity is maximized through continuous back-and-forth reflections within the DBRs through the active region. When light is reflected from a region with a low refractive index to a region with a high refractive index, a phase shift of π occurs, leading to destructive interference. When the opposite occurs, the phase shift is 2π, resulting in constructive interference, as the wave crests converge and the light increases.[18–22] The finite element method (FEM) has been used in a program to accurately and efficiently predict mode resonance. It relies primarily on a non-uniform mesh, which indicates that the computational points are distributed unevenly across different layers or regions requiring high analysis accuracy.[13,23–26] The finite element theory (FEM) is very suitable for examining optical systems and nanodevices due to its precise geometric modeling capabilities. This is due to its use of non-uniform meshes and its high accuracy at low computational costs. It is also a powerful and convenient method for calculating the mode of a 2D VCSEL.[27–30] The light propagation in the laser structure is computed by solving Maxwell's equations. A set of solutions is developed which reduce the computational load for the full resolution of specific cavity configurations. A subset of formulae, the photon rate equations, was employed to study favorable performance regimes in particular types of cavities. The interconnected optical, electrical, and thermal relationships in lasers are described by the following system of coupled rate equations, which links the dynamics of charge carriers (electrons and holes) and the dynamics of photons in the optical cavity. The study begins with the carrier rate equation, which describes the charge carrier density in the active region with respect to time.[13]

$$\frac{\partial N}{\partial t} = \frac{\eta_i I}{qV} - R_{nr}(N) - R_{sp}(N) - \nu_g g(N) S \qquad (1)$$

where $\frac{\partial N}{\partial t}$ represent the rate of carrier density change, N is the carrier density, η_i is the internal injection efficiency, I is the injection current, q is the electron charge, Vis the active region volume, R_{nr} is the non-radiative recombination rate, R_{sp} is the spontaneous recombination rate, ν_g is the group velocity, g is the material gain coefficient, S is the photon density which is given by the following Eq. (2).[13]

$$\frac{\partial S_{m,w}}{\partial t} = \left[G_{m,w} - \frac{1}{\tau_{m,w}}\right] S_{m,w} + R^{spon}_{m,w} \qquad (2)$$

where S represents the photon density it counts the possible states or positions photons may occupy at a particular frequency, t is the parity time over which the photon density is calculated, G is the typical gain,τ is the half-life of the photons, and R is the spontaneous emission rate, which is given by the

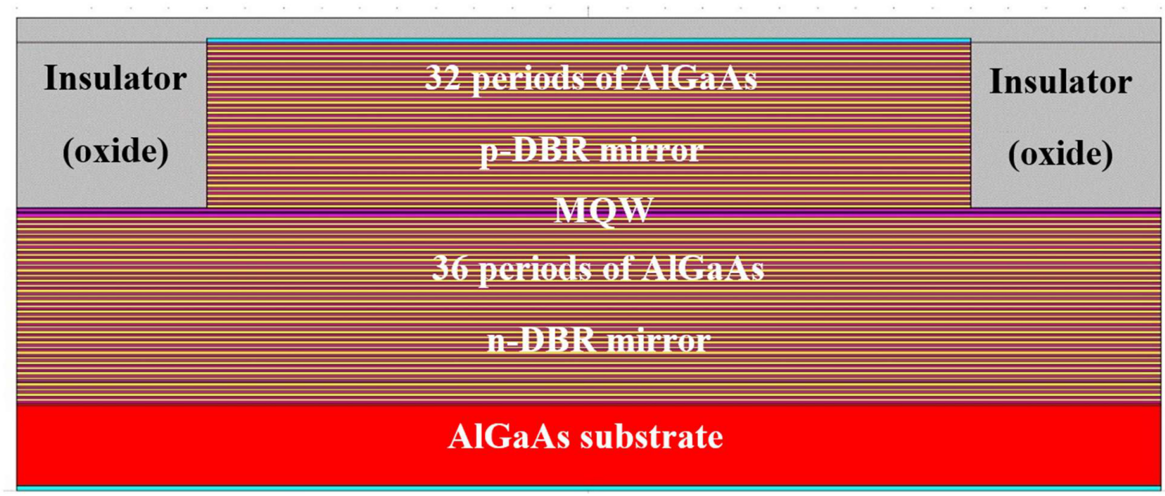

Fig. 1. Schematic structure of the VCSEL device.

following Eq. (3).[13]

$$R^{spon}_{m,w} = \int dV |E_m|^2 \, u(w) \quad (3)$$

The typical gain equation[13] is given by

$$G_{m,w=} \int dV \; |E_m|^2 \frac{C}{n_{eff}} g(w) \quad (4)$$

where g is the material gain, dv is the differential volume element, E electric field, u is the spontaneous emission spectrum, C is the speed of light in a vacuum, and n_{eff} is the effective index. Losses caused by light propagation through the cavity sides can be calculated as given by Eq. (5).[13]

$$\frac{1}{\tau_{m,w}} = \frac{1}{\tau_{mirror}} + \frac{1}{\tau_{scatter}} + \frac{C}{n_{eff,m}} \alpha_b \quad (5)$$

Where τ_{mirror} is the time constant associated with reflection loss in mirror, $\tau_{scatter}$ is the time constant associated with the dispersion process, α_b is the modal absorption coefficient, the self-heating effect is described by solving the heat flow Eq. (6).[31]

$$\left[C_L + \frac{3}{2} K_B (ne + nh)\right] \frac{\partial T}{\partial t} = \nabla \left(K_L \nabla T - \vec{S}_e - \vec{S}_h\right) + H \quad (6)$$

where C_L is the lattice heat capacity, K_B is the Boltzmann constant, n_e is the electron density, n_h is the hole density, T is the absolute temperature, t is the time, K_L is the thermal conductivity coefficient, S_e is the electronic heat source, S_h is the hole heat source, H is the heat transfer coefficient.[31] Eqs. (1) to (6) represent an approach that can help develop and improve the VCSEL model by relying on electrical and optical phenomenon.

VCSEL model

The proposed vertical cavity surface emission laser (VCSEL) is designed to operate at a wavelength of 850 nm. Fig. 1 illustrates the device core structure on an Al_0Ga_1As substrate, providing the required lattice compatibility and refractive index for the crystalline layer. The active region consists of three quantum wells (MQWs) formed using two material systems: GaAs (Eg = 1.42 ev) and $Al_{0.01}Ga_{0.99}As$ (Eg = 1.43 ev), each with a physical thickness of 0.008 μm. Each quantum well is surrounded by 0.008 μm thick $Al_{0.2}Ga_{0.8}As$ barrier layers to ensure effective vector confinement and optimize the spatial positioning of the optical field within the cavity. High-efficiency optical feedback is achieved by incorporating distributed Bragg reflectors (DBRs) arranged above and below the active region. These diopter sensing devices (DBRs) are constructed using alternating layers of $Al_{0.55}Ga_{0.45}As$ with thicknesses selected to meet the optical requirement of a quarter wavelength for constructive interference. The extra pairs in the lower mirror provide greater optical confinement and gain, which helps to maintain stable laser oscillation. An oxide layer is deposited on the top DBR and on both sides of it to further improve the performance of the device. This layer provides lateral confinement and minimises optical leakage for better cavity performance. The diameter of the oxide aperture is also chosen to be 10 μm to guarantee lateral confinement and hence better optical mode localization in the cavity. The integrated structural design of engineered QWs, high-reflectivity DBRs and an optimally positioned oxide aperture offers a well-optimized optical cavity that can deliver reliable illumination, effective carrier retention and enhanced thermal and operational durability.

Results and discussion

This study uses the finite element method to simulate the two-dimensional configuration of a vertical-cavity surface-emitting laser (VCSEL), considering the optical response light propagation characteristics of the quantum well (QW) area in the presence of two different materials: AlGaAs and GaAs. The simulation results show that both materials have almost the same optical characteristics at the design wavelength of 850 nm, and only minor distinctions are due to the material's intrinsic electronic and optical properties. The spatial profile of electrons and holes in the active region and the effect on important device parameters (such as the minimum lasing power, the bias voltage and the cavity resonance wavelength) were also analyzed. The transmission spectra of Fig. 2a and b, indicate that the AlGaAs configuration has a strong peak at around 0.871 μm, and the GaAs configuration has a peak at around 0.868 μm. These results show that these results are due to the transmission peaks of the DBR, and the small shift from the design wavelength of 850 nm is caused by using first order numerical elements and the effective refractive index of the DBR layers. Besides the small changes in the resonant wavelength, there are also lattice structure variations, directional variation of the layer properties and scattering phenomena within the cavity, which all cause a slight adjustment of the photonic mode. There is also a transmission peak in the stopband region, which marks the beginning of a resonant wavelength response due to the particular optical properties of the cavity.

The two dimensional distribution of the electromagnetic field in the selected parts of the VCSEL structure made of GaAs and AlGaAs is shown in Fig. 3. The spatial intensity pattern has a stable and well defined profile, which is consistent with the theoretical solutions of the wave-equation that describes the optical behaviour of the resonant cavity. The stability of single mode operation is ensured by the consistency of this, reflecting an efficient cavity design with high mode confinement and minimal spreading of the evanescent field. No discernable distortions or scattering signatures can be seen as well, further indicating that the emitted mode has a high degree of spatial coherence throughout the cavity. The AlGaAs configuration gives an effective refractive index of ~3.68 for the fundamental (0,0) mode, which is higher than the value of ~3.3 found for GaAs. This difference is due to the strong atomic and electronic structures of the two materials. This means that the inclusion of Al in AlGaAs increases the polarizability response of the material at local level, thus increasing the interaction with the electromagnetic field. The photon density, therefore, is higher in the AlGaAs region, which means that optical confinement is more efficient than in GaAs. The results show that the atomic-scale composition plays a key role in determining the photon distribution and controlling the fundamental electronic interactions, which allows for stronger confinement and modal stability in the laser cavity of AlGaAs.

Fig. 4 presents the LIV characteristics current, voltage and optical output of both GaAs and AlGaAs based VCSEL structures under different operating temperature. In Fig. 4a and b, the GaAs device shows a threshold current of about 0.45 mA at a threshold voltage near 1.23v at 300k, reaching a maximum

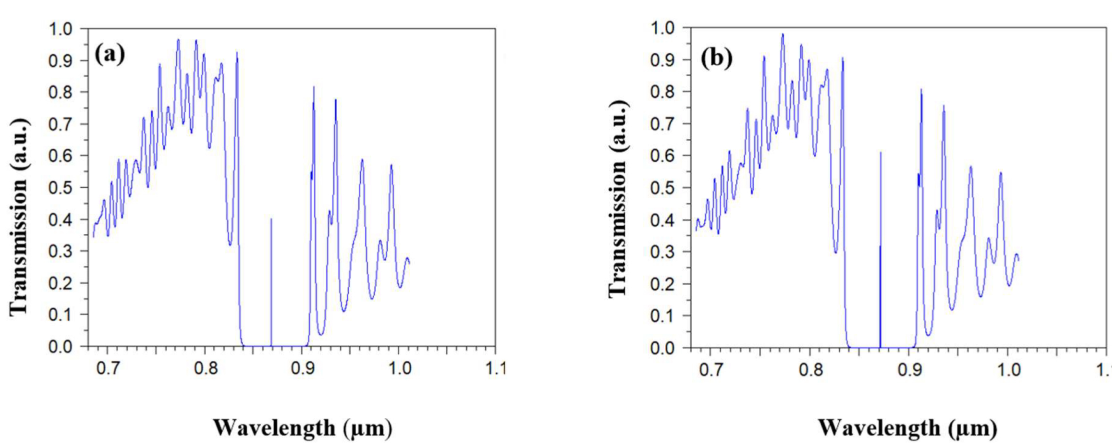

Fig. 2. Transmission spectra (at Bias0), a) GaAs, b) AlGaAs.

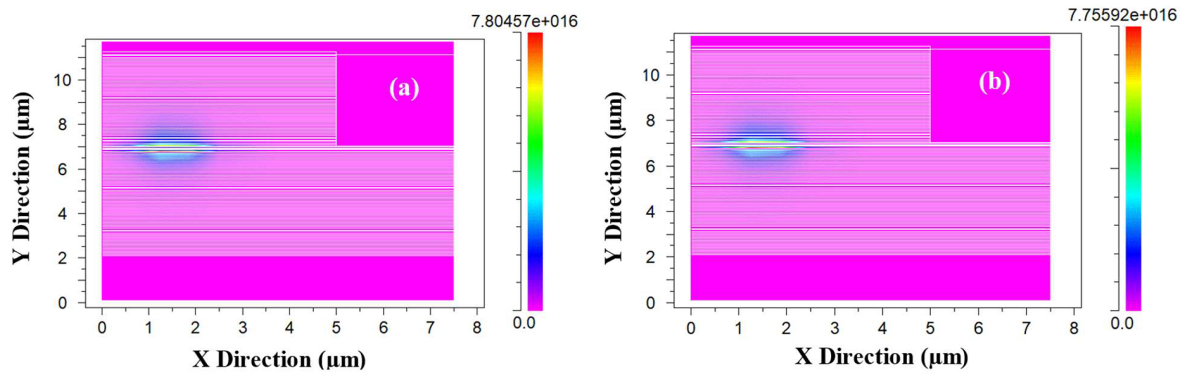

Fig. 3. Mode [0,0] (at Bias0), a) GaAs (Neff = 3.30), b) AlGaAs (Neff = 3.68).

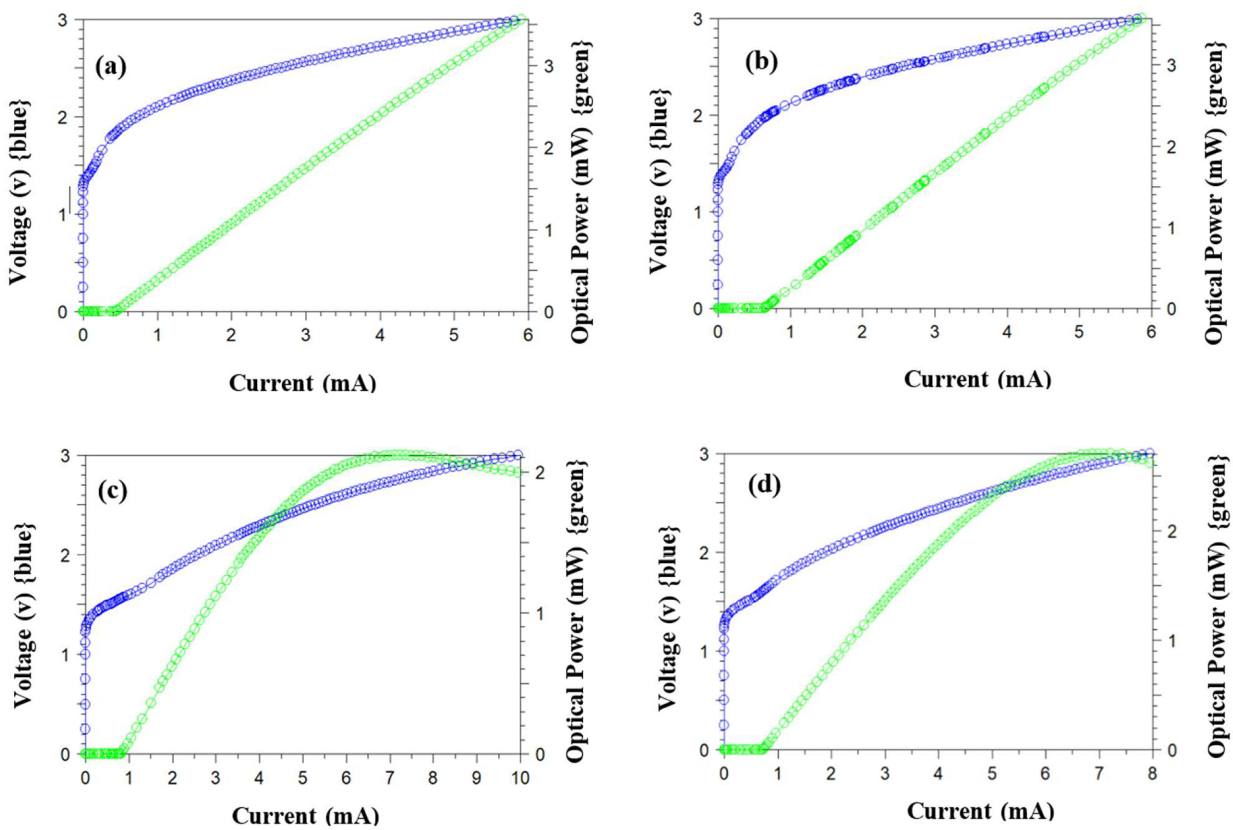

Fig. 4. Light&Voltage VS current (at T = 300k), a) GaAs, b) AlGaAs, c) GaAs (at T = 375k), d) AlGaAs (at T = 350k).

optical power of nearly 3.56 mw at around 5.9 mA. The device maintains stable behavior with no evident thermal degradation. In contrast, the AlGaAs device requires a slightly higher threshold current of about 0.67 mA, while keeping the same threshold voltage, and produces a comparable maximum output of about 3.57 mw at 5.8 mA. In Fig. 4c and d, illustrate the LIV performance at elevated temperatures. The GaAs design maintains to operate efficiently up to 375k, where the threshold current increase to around 0.62 mA and the peak output power continues stable before dropping at higher temperature according to thermal effects. While AlGaAs design operates efficiently up to 350k, where the threshold current increases to about 0.75 mA and maintains stable output power until it reaches a higher temperature, after which it begins to decrease due to the thermal effects. However, Fig. 4 demonstrate that GaAs maintains better thermal stability and optical performance over a wider temperature range, whereas AlGaAs become limited by heat buildup at lower temperature, although comparable

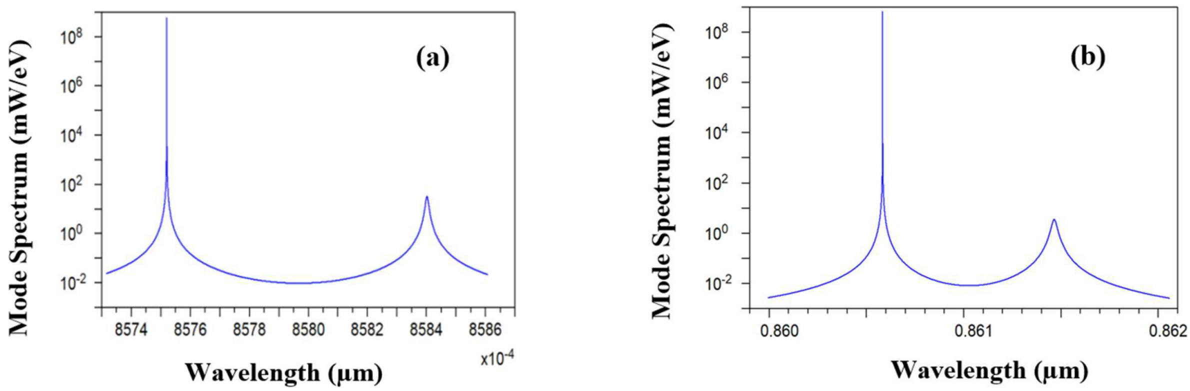

Fig. 5. Optical spectrum (at Bias7), a) GaAs, b) AlGaAs.

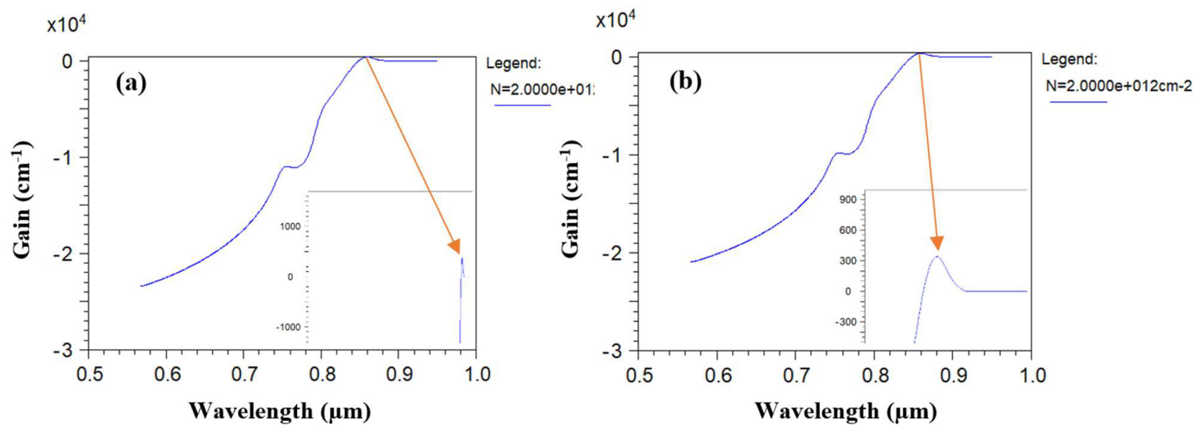

Fig. 6. Material gain, a) GaAs, b) AlGaAs.

performance at room temperature. The threshold current values reported in previous studies[6,32] over the temperature range 298–358 K are 1.5–4.1 mA and 1.55–3.70 mA, respectively. These ranges provide a reference for comparison and context for the operating characteristics of VCSEL devices.

Fig. 5 displays the optical spectrum measured at a bias 7 (3 V). In the GaAs structure, the main emission appears around 0.857 μm, while the AlGaAs structure generates a marginally shifted peak, located near 0.860–0.861 μm. This small difference in peak position cannot be explained solely by the band-gap. Instead, it mainly comes from how the distribution of the optical mode inside the cavity during operation. Variations in the effective index profile distribution, the degree of mode confinement set by the oxide aperture, and the thermal-induced variations that occur under bias all influence the resonant behavior of the cavity inside the device. Because these effects combine, the emission peak results in a small wavelength shift, reflecting the joint contribution of both the material properties and the cavity behavior.

The gain spectra of the simulated material, as seen in Fig. 6a, b, have a significantly higher gain in the range of wavelengths from 0.857 to 0.86 μm. The gain values obtained with GaAs are slightly higher than those obtained with AlGaAs, and are as high as 400 cm^{-1}, whereas the gain values obtained with AlGaAs are of the order of 350 cm^{-1}. This difference shows that the light-amplification efficiency in the active region of the GaAs based structure is higher. This difference is due to the electronic and optical characteristics of each material, including the effective mass, the density of states, the refractive index, and the elements of the moment matrix, which are responsible for radiative transitions and the effective gain in GaAs. These values are also dependent on the temperature, with higher temperatures corresponding to lower gains for both materials, from both redistribution of carriers and expansion of the energy gap due to thermal effects that slow down the rate of radiative transitions, and hence lower effective gain.

The horizontal cross-section of the electron density at bias 7(3v) in the GaAs quantum well and AlGaAs quantum well are presented in Fig. 7 a and

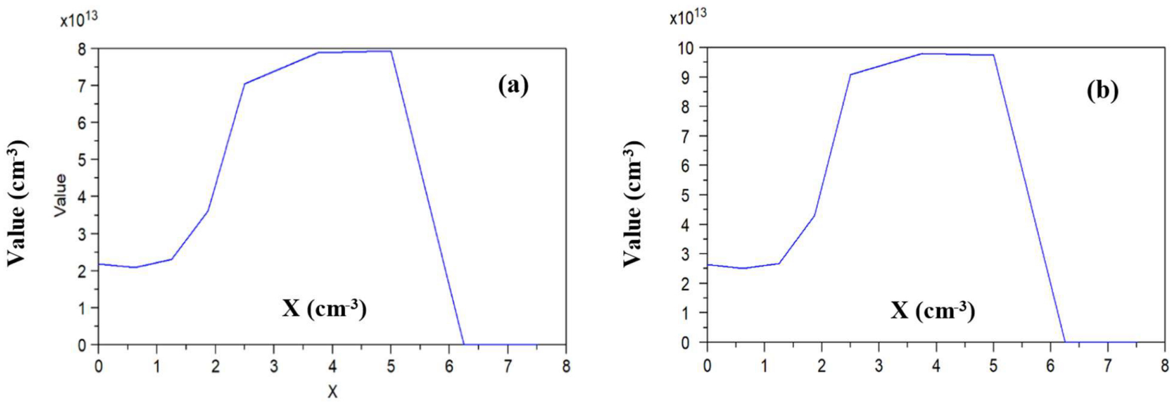

Fig. 7. Horizontal cut of electron density (cm^{-3}) (At Bias7), a) GaAs, b) AlGaAs.

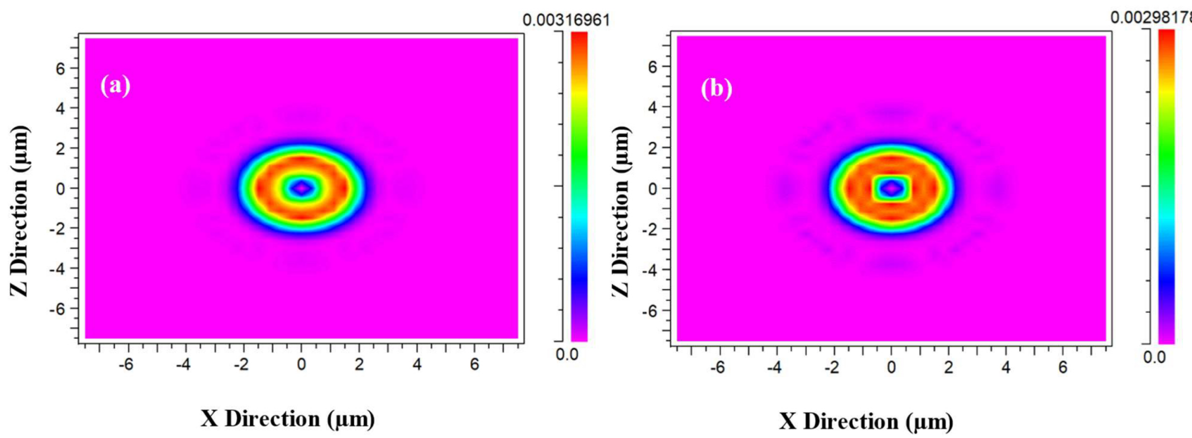

Fig. 8. Near field intensity (at Bias7) (At y = 11.2), a) GaAs, b) AlGaAs.

b, respectively. The two curves clearly show that there is a distinction in the carrier behaviour of the two materials. For the GaAs design, the electron concentration is ramped up gradually up to about 6×1013 cm^{-3}. The AlGaAs design, on the other hand, shows a steeper rise, with a concentration of almost 9×1013 cm^{-3} at the same position. This behavior is mainly correlated to the physical properties of the material. AlGaAs has a wider band-gap than GaAs, which exhibits in stronger carrier confinement and higher potential barriers at the quantum well interfaces. This tighter confinement results in electrons having less freedom to spread laterally, making the curve sharper and more concentrated in the center.On the other hand, GaAs allows for smoother diffusion of carriers, which results in a broader distribution. The introduction of aluminum increases the energy barrier around the active region. Reducing the movement of electrons out of the well. Therefore, the AlGaAs structure demonstrates a stronger optical confinement and higher carrier concentration, while the GaAs structure presents a more gradual distribution.

Figs. 8 and 9 display the spatial distribution of the optical field intensity for two VCSEL structures—a, GaAs and b, AlGaAs—operating at a bias of 7, which was extracted by taking a cross-section at the spatial coordinate Y = 11.2 μm. The figures highlight the beam characteristics in both the far-field (angular space) and near-field (physical space) regimes. Fig. 8a, b, gives the intensity distribution in the near-field at the aperture of the emitter. The AlGaAs quantum-well structure exhibit a smaller mode field diameter (MFD) for approximately 3.5 um while the GaAs design shows of about 4.0 μm. The reduction in the MFD for the AlGaAs device indicates stronger optical confinement, which obtained from the higher refractive-Index contrast between the well and its surrounding layers. This enhanced optical confinement. In AlGaAs design and reduces the lateral spreading of the mode, in addition maintains the optical field more concentrated around the beam waist. On the other hand, a smaller near-field spot is leading to a narrower far-field divergence. Hence the AlGaAs device exhibits a divergence angle of about 18°, while

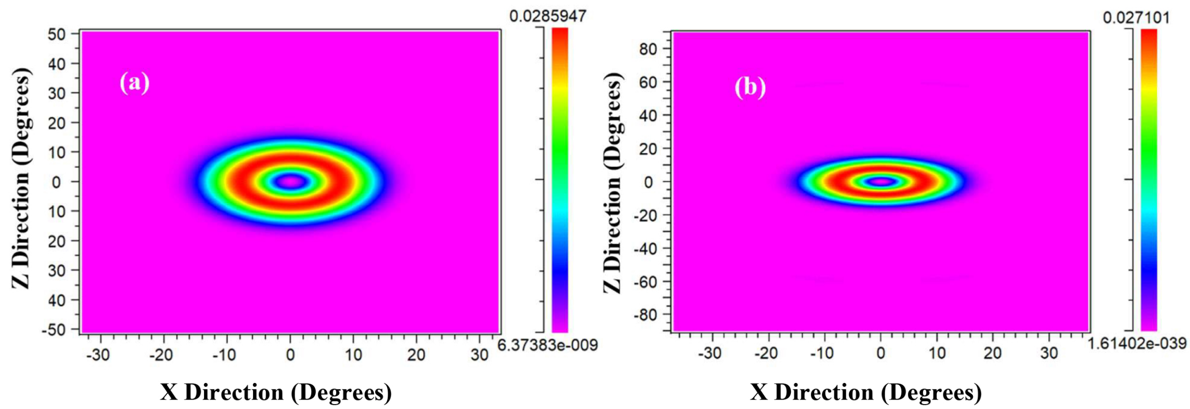

Fig. 9. Far field intensity (at Bias7) (At y = 11.20), a) GaAs, b) AlGaAs.

Table 1. Comparative analysis: GaAs QW vs AlGaAs QW with physical interpretation.

Property	GaAs QW (Description + Physical Interpretation)	AlGaAs QW (Description + Physical Interpretation)
Main Lasing Wavelength	GaAs QW: ∼0.8575 μm. Interpretation: lower effective refractive index → shorter wavelength emission.	AlGaAs QW: ∼0.860–0.861 μm. Interpretation: higher effective refractive index → longer wavelength despite larger bandgap.
Threshold Current	GaAs QW: I_{th} = 0.45 mA Interpretation: Due to higher visual gain.	AlGaAs QW: I_{th} = 0.67 mA Interpretation: Due to lower visual gain.
Optical Confinement	GaAs QW: Weaker confinement. Interpretation: Lower refractive index contrast reduces field localization.	AlGaAs QW: Stronger confinement. Interpretation: Higher refractive index contrast enhances localization of the optical mode.
Effective Index (Neff)	GaAs QW: ∼3.30. Interpretation: Lower effective index → broader mode profile.	AlGaAs QW: ∼3.68. Interpretation: Higher Neff → stronger confinement & better mode overlap.
Thermal Stability	GaAs QW: It work stably until 375k Interpretation: Higher thermal conductivity.	AlGaAs QW: The self-heating effect is evident when 350k Interpretation: Lower thermal conductivity.
Optical Gain	GaAs QW: 400 cm^{-1} Interpretation: Higher carrier confinement.	AlGaAs QW: 350 cm^{-1} Interpretation: Lower carrier confinement.
Mode Field Diameter(μm) Divergence Angle(°)	GaAs QW:4.0μm, 24° Interpretation: Less optical confinement and lower effective refractive index.	AlGaAs QW:3.4μm, 18° Interpretation: Stronger optical confinement and higher effective refractive index.

the GaAs device demonstrates a wider divergence of nearly 24° due to its weaker confinement.

Table 1 shows the important optical properties of GaAs and AlGaAs quantum wells in a VCSEL at a wavelength of 850 nm, showing the effect of both the effective refractive index and carrier retention on the emission wavelength and optical gain.

Conclusion

This study utilized the Laser MOD of RSoft software to simulate and analyze the performance of a two-dimensional vertical-cavity surface-emitting laser (VCSEL) array for integration into modern optical data communication systems. Comparative FEM simulations at a wavelength of 850 nm were conducted. The quantum wells of the GaAs structure provided better optical gain, lower ripple current, and higher thermal stability compared to AlGaAs in the same cavity design. GaAs exhibited stable performance up to 375 K, while the AlGaAs structure deteriorated at lower temperatures, showing self-heating around 350 K due to its lower thermal conductivity. On the other hand, AlGaAs offers high optical excitability due to its high effective refractive index, which promotes better mode localization in the active region. The results demonstrate the significance of taking into account the optical properties of QW materials, including gain and confinement, when designing a VCSEL. The analysis done in the present study is based on two-dimensional numerical simulation to account for the dominant optical and thermal characteristics of VCSEL operation under the design parameters considered. This allows an efficient evaluation of material and cavity effects but does not explicitly solve 3D field distributions, fabrication variations or higher order carrier transport phenomena.

Future work will include full 3-D modeling and a more detailed understanding of carrier dynamics, which will help to better understand device behavior, especially at high current and high temperature, in a more quantitative way.

Authors' declaration

- Conflicts of Interest: None.
- We hereby confirm that all the Figures and Tables in the manuscript are ours. Furthermore, any Figures and images that are not ours have been included with the necessary permission for re-publication, which is attached to the manuscript.
- No animal studies are present in the manuscript.
- No human studies are present in the manuscript.
- Ethical Clearance: The project was approved by the local ethical committee at University of Baghdad.

Authors' contributions statement

R. M. K. conducted the theoretical simulation of the 2D VCSEL using the FEM theory in the RSoft Laser MOD program. S. S. M. supervised the research and provided guidance and instructions.

References

1. Gullino A. Physics-based modeling of 850 nm tunnel junction VCSELs [dissertation]. Torino: Politecnico di Torino; 2023 [cited 2025 Feb 12].
2. Naim NF, Hashim MAH, Sarnin SS, Ya'acob N, Supian LS. Design of L-band multiwavelength laser for TDM/WDM PON application. Baghdad Sci J. 2021;18(4 Suppl.):1365-70. http://doi.org/10.21123/bsj.2021.18.4(Suppl.).1365
3. Mahdi SS, Hamad IA. A laser induced fluorescence design for renewable energy application. Karbala International Journal of Modern Science. 2020;6(3): Article 9. https://doi.org/10.33640/2405-609X.1707
4. Gullino A, Tibaldi A, Bertazzi F, Goano M, Debernardi P. Reduced dimensionality multiphysics model for efficient VCSEL optimization. Appl Sci (Basel). 2021;11(19):6908. http://doi.org/10.3390/app11156908
5. Shang J, Cong C, Wang Z, Peimyoo N, Wu L, Zou C, *et al.* Room-temperature 2D semiconductor activated vertical-cavity surface-emitting lasers. Nat Commun. 2017;8:543. http://doi.org/10.1038/s41467-017-00743-w
6. Cheng H-T, Yang Y-C, Liu T-H, Wu C-H. Recent Advances in 850 nm VCSELs for High-Speed Interconnects. Photonics. 2022; 9(2): 107. https://doi.org/10.3390/photonics9020107
7. Khidhir AH. Optimum diameter for laser beam and effect of temperature rise on the optical bistability hysteresis loops. Iraqi J Phys. 2020;18(45):32-9. http://doi.org/10.30723/ijp.v18i45.520
8. Tibaldi A, Bertazzi F, Goano M, Michalzik R, Debernardi P. VENUS: a vertical-cavity surface-emitting laser electro-opto-thermal numerical simulator. IEEE J Sel Top Quantum Electron. 2019;25(6):1500212. http://doi.org/10.1109/JSTQE.2019.2893755
9. Yu TC, Huang WT, Wang HC, Chiu AP, Kou CH, Hong KB, *et al.* Design and simulation of InGaN-based red vertical-cavity surface-emitting lasers. Micromachines (Basel). 2024;15(1):87. http://doi.org/10.3390/mi15010087
10. Dua S, Su J, Zhou H, Zhang H, Qiu P, Deng J, *et al.* Temperature-dependent characteristics of the high-speed 850 nm VCSEL. Proc SPIE. 2024;13183:1318309. http://doi.org/10.1117/12.3033973
11. Pomplun J, Burger S, Schmidt F, Schliwa A, Bimberg D, *et al.* Finite element simulation of the optical modes of semiconductor lasers. Phys Status Solidi B. 2010;247(4):846-53. http://doi.org/10.1002/pssb.200945451
12. Arabi NA, Jaber GN. Bandwidth improvement of a cone-inverted cylindrical and cross hybrids dielectric resonator antennas. Iraqi J Phys. 2023;21(1):77-87. http://doi.org/10.30723/ijp.v21i1.1084
13. Agrawal GP, Dutta NK. Semiconductor Lasers. 2nd ed. New York: Van Nostrand Reinhold; 1993. ISBN: 9780442011024.
14. De Leonardis F, Passaro VMN, Magno F. Improved simulation of VCSEL distributed Bragg reflectors. J Comput Electron. 2007;6(3):289-92. http://doi.org/10.1007/s10825-006-0121-7
15. Xiao Y, Miao P, Wang J, Liu H, Gou Y, Zhang Z, *et al.* Twenty-milliwatt, high-power, high-efficiency, single-mode, multi-junction vertical-cavity surface-emitting lasers using surface microstructures. Photon Res. 2024;12(9):1899-907. http://doi.org/10.1364/PRJ.521098
16. Li J, Zhao J, Gao F. Numerical investigation of optical and photoelectric properties for 850 nm VCSELs with arbitrary crystal orientation. Crystals. 2022;12(10):1459. http://doi.org/10.3390/cryst12101459
17. Li MJ, Li KM, Chen X, Mishra SK, Juarez AA, Hurley JE, *et al.* Single-mode VCSEL transmission for short reach communications. J Lightwave Technol. 2020;38(15):4292-9. http://doi.org/10.1109/JLT.2020.3028972
18. Ledentsov NN, Makarov O, Shchukin VA, Kalosha VP, Ledentsov N Jr, Chorchos Ł, *et al.* High speed VCSEL technology and applications. J Lightwave Technol. 2022;40(6):1749-63. http://doi.org/10.1109/JLT.2022.3149372
19. Ii X, Zhou Y, Zhang X, Zhang J, Zeng Y, Ning Y, *et al.* High-power single-mode 894 nm VCSELs operating at high temperature (> 2 mW @ 365 K). Appl Phys B. 2022;128(1):16. http://doi.org/10.1007/s00340-021-07748-w
20. Meng Xun, Guanzhong Pan, Yun Sun, Xiaoli Zhou, Yinuo Wang, Yang Liu, *et al.* Longitudinal Multi-Cavity Coupled VCSELs With Narrow Linewidth and High Single Mode Power for Quantum Sensing. J Lightwave Technol. 2024;42(17):5949-5955. https://doi.org/10.1109/JLT.2024.3403884
21. Dąbrówka D, Sarzała RP. Study on bottom distributed Bragg reflector radius and electric aperture radius on performance characteristics of GaN-based vertical-cavity surface-emitting laser. Materials (Basel). 2024;17(13):3107. http://doi.org/10.3390/ma17133107
22. Zaccaria C, Mancinelli M, Pavesi L. A FEM enhanced transfer matrix method for optical grating design. J Lightwave Technol. 2021;39(11):3521-30. http://doi.org/10.1109/JLT.2021.3067153
23. Wang C, Li C, Dai J, Lan T, Zhou G, Meng J, *et al.* Thermal analysis of VCSEL arrays based on first principle theory and finite element method. Opt Quantum Electron. 2019;51:196. http://doi.org/10.1007/s11082-019-1909-6
24. Pomplun J, Burger S, Rozova M, Zschiedrich L, Schmidt F. Finite element simulation of optical modes in VCSELs. In: Proceedings of the 11th International Conference on Numer-

ical Simulation of Optoelectronic Devices (NUSOD); 2011. p. 119-20. http://doi.org/10.1109/NUSOD.2011.6087324
25. Dohle R, Henning G, Wallrodt M, Gréus C, Neumeyr C. Advanced packaging technology for novel 1-dimensional and 2-dimensional VCSEL arrays. Microelectron. 2021;1:000265. http://doi.org/10.1085/8024-2021-1-000265
26. Rozova M, Pomplun J, Zschiedrich LW, Schmidt F, Burger S. 3D finite element simulation of optical modes in VCSELs. Proc SPIE. 2012;8255:82550K. http://doi.org/10.1117/12.906372
27. Chen L, Zhang Y, Wang H, *et al.* Performance analysis of AlGaAs/GaAs VCSELs for optical communication. Appl Sci (Basel). 2024;14(3):2005. http://doi.org/10.3390/app14032005
28. Zhao L, Shang Q, Li M, *et al.* Strong exciton-photon interaction and lasing of two-dimensional transition metal dichalcogenide semiconductors. Nano Res. 2021;14:1937-55. http://doi.org/10.1007/s12274-020-3073-5
29. Nihui Z, Zhenjiao S, Fansheng M, Di X, Hai W, *et al.* Scaled-up 2D solid-state laser array. Opt Lett. 2025;50:2679-82. http://doi.org/10.1364/OL.554966
30. Shunya A, Zhan S, Gouen W, Shoujie Y, Fuyi C, *et al.* Single-crystal CsPbBr3-based vertical cavity surface emitting laser. Opt Lett. 2025;50:702-5. http://doi.org/10.1364/OL.547212
31. Weng C, Zhang X, Li Y. Self-heating effects in semiconductor lasers: A theoretical model. J Appl Phys. 2016;119(15):153102. http://doi.org/10.1063/1.4946002.
32. Chaqmaqchee FA, Lott JA. Impact of oxide aperture diameter on optical output power, spectral emission, and bandwidth for 980 nm VCSELs. OSA Continuum. 2020;3(9):2602–2613. http://doi.org/10.1364/OSAC.397687

نمذجة وتحليل أداء ليزر الباعث من التجويف العمودي ثنائي الأبعاد (VCSEL) باستخدام المحاكاة بالعناصر المنتهية

رند مهدي خضير[1]، شيماء صالح مهدي[2]

قسم الفيزياء، كلية العلوم للبنات، جامعة بغداد، محافظة بغداد، العراق

الخلاصة

تُعد ليزرات التجويف العمودي ذات الانبعاث السطحي (VCSELs) مكونًا أساسيًا في أنظمة الاتصالات الضوئية قصيرة المدى. ويعود استخدامها في هذه الأنظمة إلى بنيتها المدمجة، وانخفاض تيار العتبة، وقدرتها العالية على التضمين، وكفاءتها العالية. تقدم هذه الدراسة محاكاة عددية ثنائية الأبعاد لبنية VCSEL عند طول موجي مقداره 850 نانومتر باستخدام طريقة العناصر المحددة (FEM) من خلال برنامج Laser MOD، وذلك لدراسة تأثير استخدام مادتين مختلفتين للآبار الكمية (QW)، وهما GaAs وAlGaAs، على الأداء البصري للجهاز. وقد تم تنفيذ جميع ما سبق ضمن نفس بنية التجويف ومرايا DBR لضمان إجراء مقارنة متسقة. تشير النتائج إلى أن الكسب البصري لمادة GaAs أعلى، حيث يبلغ حوالي 400 cm^{-1}، مقارنةً بمادة AlGaAs التي تمتلك كسبًا بصريًا أقل يبلغ حوالي 350 cm^{-1}. كما تعمل مادة GaAs عند تيار عتبة أقل يقارب 0.45 mA، في حين أن مادة AlGaAs تعمل عند تيار عتبة يبلغ 0.67 mA. ويُظهر التحليل الحراري أن تأثير التسخين الذاتي يبدأ عند درجة حرارة أقل في بنية AlGaAs، حوالي 350 K، مقارنةً بـ GaAs التي يمكنها العمل باستقرار حتى درجة حرارة تقارب 375 K بسبب موصليتها الحرارية الأعلى. وبشكل عام، توضح المقارنة التوازن بين الأداء والكسب والحصر البصري للمادتين تحت نفس الظروف البنائية والحرارية.

الكلمات المفتاحية: عاكس براج الموزع (DBR)، طريقة العناصر المحدودة (FEM)، شدة المجال القريب، قدرة الوضع البصري، البئر الكمي.